Energy Reports 6 (2020) 147–159

Contents lists available at ScienceDirect

Energy Reports

journal homepage: www.elsevier.com/locate/egyr

Research paper

Thermodynamic analysis of high-temperature pumped thermal energy storage systems: Refrigerant selection, performance and limitations

Abdelrahman H. Hassan [a,b], Laura O'Donoghue [a], Violeta Sánchez-Canales [a], José M. Corberán [a], Jorge Payá [a,*], Henning Jockenhöfer [c]

[a] Instituto Universitario de Investigación en Ingeniería Energética, Universitat Politècnica de València, 46022, Valencia, Spain
[b] Mechanical Power Engineering Department, Faculty of Engineering, Zagazig University, Zagazig 44519, Egypt
[c] German Aerospace Center (DLR), Institute of Engineering Thermodynamics, Pfaffenwaldring 38, 70569, Stuttgart, Germany

ARTICLE INFO

Article history:
Received 19 February 2020
Received in revised form 29 April 2020
Accepted 10 May 2020
Available online 15 May 2020

Keywords:
High-temperature heat pump
Organic Rankine cycle
Thermal energy storage system
Modelling
Refrigerants

ABSTRACT

One of the bottlenecks for a wider implementation of renewable energies is the development of efficient energy storage systems which can compensate for the intermittency of renewable energy sources. Pumped thermal energy storage (PTES) is a very recent technology that can be a promising site-independent alternative to pumped hydro energy storage or compressed air energy storage, without the corresponding geological and environmental restrictions. Accordingly, this paper presents a full thermodynamic analysis of a PTES system consisting of a high-temperature heat pump (HTHP), which drives an organic Rankine cycle (ORC) by means of an intermediate high-temperature thermal energy storage system (HT-TES). The latter combines both latent and sensible heat thermal energy storage sub-systems to maximize the advantage of the refrigerant subcooling. After validating the proposed model, several parametric studies have been carried out to assess the system performance using different refrigerants and configurations, under a wide range of source and sink temperatures. The results show that for a system that employs the same refrigerant in both the HTHP and ORC, and for a latent heat thermal energy storage system at 133°C, R-1233zd(E) and R-1234ze(Z) present the best performance. Among all the cases studied with a latent heat thermal energy storage system at 133°C, the best system performance, also considering the impact on the environment, has been achieved employing R-1233zd(E) in the HTHP and Butene in the ORC. Such a system can theoretically reach a power ratio of 1.34 under HTHP source and ORC sink temperatures of 100 and 25°C, respectively.

1. Introduction

Global warming and pollution are nowadays among the main concerns which are being addressed by energy strategies. The European Union has set the following targets for 2030: to reach a 40% reduction in greenhouse gas emissions (with respect to the levels in 1990), to reach a share of at least 27% in renewable energies with regards to energy generation and to reach a global efficiency of at least 30% in the entire European Union (European Comission, 2018; European Council, 2014).

Integrating renewable energy sources (RES) with energy storage systems can play a significant role in reducing the global carbon footprint. The intermittency of renewable energies can be overcome, if more efficient energy storage systems are developed and integrated into the grid (Aneke and Wang, 2016; BP plc, 2018).

Taylor et al. (2012) recently compared different electrical energy storage systems. Among the possible large-scale electricity storage technologies, up-to-date none is fully feasible from a technical, economical and an environmental point of view. Storage with batteries, for instance, is currently not available for large-scale electricity storage (more than 50 MW), and furthermore, their long-term performance still has to be improved, as well as some environmental issues related to the waste components.

Pumped hydro energy storage (PHES) is by far the most mature and widely utilized energy storage technique, as it accounts for around 99% of the global large scale energy storage systems (Aneke and Wang, 2016). PHES employs the excess electricity to pump water to an upper reservoir (lakes, caves, etc.) and produces electricity when needed by driving this water through a turbine. Fan et al. (2020) recently indicated that the proposed system can have an average theoretical efficiency of around 82.8%. A micro-PHES study was presented by Kusakana (2019). The author

* Corresponding author.
E-mail address: jorge.paya@iie.upv.es (J. Payá).

https://doi.org/10.1016/j.egyr.2020.05.010

Nomenclature

COP	Coefficient of Performance [–]
C_p	Specific heat [J kg^{-1} K^{-1}]
h	Enthalpy [J kg^{-1}]
m	Mass flow rate [kg s^{-1}]
P	Pressure [Pa]
PE	Electrical power [W]
Pr	Pressure ratio [–]
Q	Thermal power [W]
s	Entropy [J kg^{-1} K^{-1}]
SC	Subcooling [K]
SH	Superheat [K]
T	Temperature [°C]
VHC	Volumetric heat capacity [J m^{-3}]
x	Dryness fraction/quality [–]
Δh_{fs}	Enthalpy of fusion/solidification [J kg^{-1}]
ΔT	Temperature difference [K]
ΔT_{PP}	Pinch point inside heat exchangers [K]
η	Efficiency [–]
φ	Net power ratio [–]
ν	Specific volume [m^{-3} kg^{-1}]

Subscripts

comp	Compressor
cond	Condenser
crit	Critical
dis	Discharge
evap	Evaporator
exp	Expander
HTHP	High-temperature heat pump
is	Isentropic
lat	Latent
LH-TES	Latent heat thermal energy storage
ORC	Organic Rankine cycle
PCM	Phase change material
PH	Preheater
pump	Pump
r	Refrigerant
sat	Saturated
SC	Subcooler
sen	Sensible
snk	Heat sink
src	Heat source
suc	Suction
th	Thermal
tot	Total
w	Water

proposed a numerical model to manage and operate a 2 kW wind pump with pico hydro generator and a borehole in pumped hydro storage configuration. The resulted showed that up to 63.62% can be saved on the cost of energy consumed using the proposed micro-PHES system compared to the direct grid supply. However, geological constraints and site availability are the main eco-environmental challenges that can face the implementation of PHES systems, especially in megawatts-scale (Budt et al., 2016; Ma et al., 2014).

Compressed air energy storage (CAES) is one of the thermo-mechanical storage techniques based on transformations between mechanical and thermal energy. The main concept consists in converting the electric energy to mechanical energy by means of electrically driven air compressors. The pressurized air produced can be stored in natural caverns under the ground or artificial reservoirs. At high demand periods, the air is reheated and expanded through an expander attached to the generator in order to produce electricity (Budt et al., 2016). Giovannelli et al. (2019) investigated the possibility of using conventional steam turbines as air expanders for small/medium-scale CAES systems (1–10 MW). In the authors' opinion this could be a good reference to reduce development efforts and costs. Regarding small-scale CAES applications, Cheayb et al. (2019) presented a steady-state thermodynamic modelling of a small-scale trigenerative-CAES (T-CAES) system. The authors stated that the proposed system has a low roundtrip efficiency of 15.6%. The main drawbacks of conventional CAES systems are the low roundtrip efficiency, and the reheating of air required before the expansion process by combusting fossil fuels. However, the negative environmental impact of conventional CAES systems can be mitigated by using the adiabatic-CAES concept (Liu and Wang, 2016).

To overcome the drawbacks of PHES and CAES techniques, the PTES concept was proposed (Abarr et al., 2017a; McTigue et al., 2015; Steinmann, 2017, 2014). PTES is mainly a thermo-mechanical energy storage technique in which the excess electricity from RES is used to create a temperature difference between two heat reservoirs. During the discharge process, this temperature difference is used to drive a heat engine cycle to generate electricity on demand. There are many classifications for PTES systems based on the thermodynamic cycles employed in the charging and discharging processes, such as PTES-Brayton cycle, PTES-CO_2 cycle, PTES-Rankine (organic Rankine) cycle, etc. (Steinmann, 2017).

Steinmann (2017) compared the previous alternatives (PHES, CAES, and PTES) for electricity storage regarding their applicability, cost, and efficiency. He indicated that PTES is the most promising technology compared to the other options. Among other advantages of this alternative, a very relevant one is that it can theoretically reach a 100% roundtrip efficiency (ratio between output and input electrical power). The author emphasized that although most of the components for these thermal storage concepts are already available, many of them still need improvements and modifications to meet the requirements regarding efficiency and operating temperatures.

Research in the field of PTES including thermal energy storage is mostly theoretical. Thess (2013) developed a simplified thermodynamic model to predict the global performance of PTES. Another thermodynamic analysis for a PTES system based on Joule cycle in charging and discharging was presented by McTigue et al. (2015). The authors revealed that by using an "optimistic" set of loss parameters and efficiencies, that might be achievable with reciprocating devices, the thermodynamic round-trip efficiency of the proposed system could exceed 85% whilst the system simultaneously achieves an energy density almost an order of magnitude greater than that for CAES.

Guo et al. (2016) indicated that there is an optimum value for the thermal energy storage temperature that gives the maximum roundtrip efficiency for PTES systems. Thus, to achieve the best performance, such systems should be controlled to work in the region below or equal to this optimum temperature.

Abarr et al. (2017a,b) presented a detailed model of PTES system coupled with a natural gas turbine powered plant using a tube-in-concrete HT-TES, such system is called "Bottoming-PTES". The proposed system was based on a transcritical ammonia cycle for both the charging and discharging processes. The simulation results, based on the baseline inputs, showed stand-alone energy storage efficiencies between 51 and 66%, and a stand-alone bottoming efficiency of 24%. Laughlin (2017) theoretically

analysed PTES-Brayton cycle systems and stated that they have the possibility to reach a theoretical roundtrip efficiency of 75%.

The current work mainly focuses on the PTES-Rankine (organic Rankine) cycle concept which is also known as Compressed Heat Energy STorage (CHEST) (Jockenhöfer et al., 2018; Steinmann et al., 2019; Steinmann, 2017, 2014). This system has the advantage that it is based on already available and mature technologies which could in principle be specifically designed to reach higher roundtrip efficiencies than the previous alternatives; besides, the CHEST system does not have geological constraints or harmful impacts on the environment, especially if the working fluids are selected properly.

In the CHEST concept the excess electricity is used during the charging process to drive a HTHP which pumps the energy from a low-temperature heat source (e.g. seasonal pit water heat storage, waste industrial heat, etc.) to a high-temperature heat sink (thermal energy storage system). Later, the stored energy can be used to power an ORC and hence produce electrical power in periods of high demand, or fit the electricity generation to a given demand. To the best of our knowledge, the CHEST concept has only been analysed theoretically up-to-date and there are no experimental installations yet.

One of the first thermodynamic studies of CHEST systems was performed by Steinmann (2014), who presented a thermodynamic and theoretical analysis of some configurations and techniques used for CHEST systems. The proposed system can reach a 72.8% roundtrip efficiency and even higher than 100% if the CHEST system is integrated with a low-temperature heat source of 88 °C or more.

Frate et al. (2017) developed a numerical model for the CHEST system consisting of a vapour-compression HP and ORC, using low-temperature heat sources between 80 and 110 °C to reach a roundtrip efficiency beyond 100%. In this work several refrigerants were analysed, bearing in mind their environmental impact to discard those that do not comply with the European legislation. Among the studied refrigerants, R-1233zd(E) seems to be the most promising one, reaching a maximum roundtrip efficiency of 130% at a source temperature of 110 °C. Moreover, R-1233zd(E) showed the lowest operational pressure ratio of 2, for a source temperature of 80 °C, compared with other fluids.

Jockenhöfer et al. (2018) presented the most recent and detailed model for the CHEST system coupled with low-temperature heat sources. Firstly, the authors discussed the potential working fluids for the HTHP and ORC, focusing on the effect of the saturated vapour slope on the system performance. They chose to use Butene, an isentropic fluid (fluid that has an almost vertical saturated vapour line on the T-s diagram). The proposed model takes into account pinch points and pressure drops inside the heat exchangers, different source and sink temperatures, and efficiencies of different equipment (compressor, pumps, and expander). The main modelling assumptions were that the liquid at the exit of the ORC's preheater is saturated, and that the sensible to latent heat ratio is the same for both charging and discharging. To prevent the flash vapour generation during the expansion process and to increase the evaporator capacity, the authors adopted an excess heat exchanger after the HTHP's subcooler. The results showed that for a sink temperature of 15 °C, a source temperature of 100 °C and a pinch point of 5 K inside the heat exchangers, the system can reach a net roundtrip efficiency of 125%. The same research group has recently presented different operation modes with the CHEST system for smart management of electricity and heat (Steinmann et al., 2019).

The present paper is an extensive thermodynamic analysis of the CHEST system including the basic components, refrigerants, and configurations. The main novelties in the current study compared to the previously published literature (Jockenhöfer et al., 2018; Steinmann et al., 2019) are:

(i) for the first time, different CHEST system configurations (with and without excess heat) have been compared to find the maximum theoretical performance;
(ii) different combinations of refrigerants and heat storage temperatures have been analysed to make an integral analysis of the system; and finally
(iii) the possibility of using different working fluids in the HTHP and ORC has been explored for the first time, and the expected improvements on the CHEST system performance are discussed.

2. CHEST system concept and components

2.1. System configuration and theoretical analysis

Fig. 1 shows the general layout of the CHEST system. In the charging cycle (left cycle) the HTHP pumps the heat ($Q_{src,HTHP}$) from a low-temperature heat source and stores it in the HT-TES system. Firstly, the thermal energy is stored as latent heat in the latent heat thermal energy storage (LH-TES) unit during the condensation of the refrigerant (2→3). Secondly, the sensible heat thermal energy storage (SH-TES) unit recovers additional heat owing to the subcooling of the refrigerant (3→4). Finally, the refrigerant is expanded (4→5) to close the cycle.

During periods of high electricity demand, the discharging cycle (right in Fig. 1) is employed. Firstly, the stored sensible heat is used to preheat the refrigerant (7→8). Secondly, its evaporation is achieved inside the LH-TES, reaching the outlet as superheated vapour (8→9). Thirdly, the refrigerant expands (9→10) to produce electrical power. Finally, the condenser (10→6) returns the refrigerant to a liquid state before it is pumped (6→7) again to close the cycle.

The CHEST system is theoretically a very flexible system, especially if it is coupled with a smart district heating (SDH) system as shown in Fig. 2 (Steinmann et al., 2019). In summer, for example, the electrical energy demand is high, mainly for air-conditioning and refrigeration applications, unlike the district heating demand. In this scenario the CHEST system can use the excess solar energy to reduce the compressor consumption during the charging cycle. In the discharging cycle, the CHEST system operates mainly to produce electrical energy, and the rejected heat portion could be used to charge the seasonal thermal storage (upper part of Fig. 2). Contrarily, in winter the district heating demand is elevated and wind energy is more available than solar energy. To satisfy this situation, the CHEST system could employ wind energy to charge the HT-TES, and later during the discharging process, a smaller portion of stored energy could be converted into electricity, while, a major part could be injected as heat into the SDH system (lower part of Fig. 2).

2.1.1. HTHP analysis

The HTHPs are usually referred to as industrial heat pumps, especially for waste heat recovery. Arpagaus et al. (2018) defined the limits of heat sink temperature for HTHP applications as between 100 and 160 °C. The majority of HTHPs are related to closed-cycle compression heat pumps, as this type is available in many sizes for different applications (Arpagaus et al., 2018).

The HTHP's evaporator capacity, or the heat absorbed from the low-temperature heat source, ($Q_{src,HTHP}$) is calculated as:

$$Q_{src,HTHP} = m_{r,HTHP}\,(h_1 - h_5) = m_{src,HTHP} \cdot Cp_{src,HTHP} \cdot \Delta T_{src,HTHP} \quad (1)$$

The total electrical power consumed by the compressor is evaluated as shown in Eq. (2), considering the total compressor efficiency $\eta_{tot,comp,HTHP}$.

$$PE_{comp,HTHP} = \frac{m_{r,HTHP}\left(h_{2,is} - h_1\right)}{\eta_{tot,comp,HTHP}} \quad (2)$$

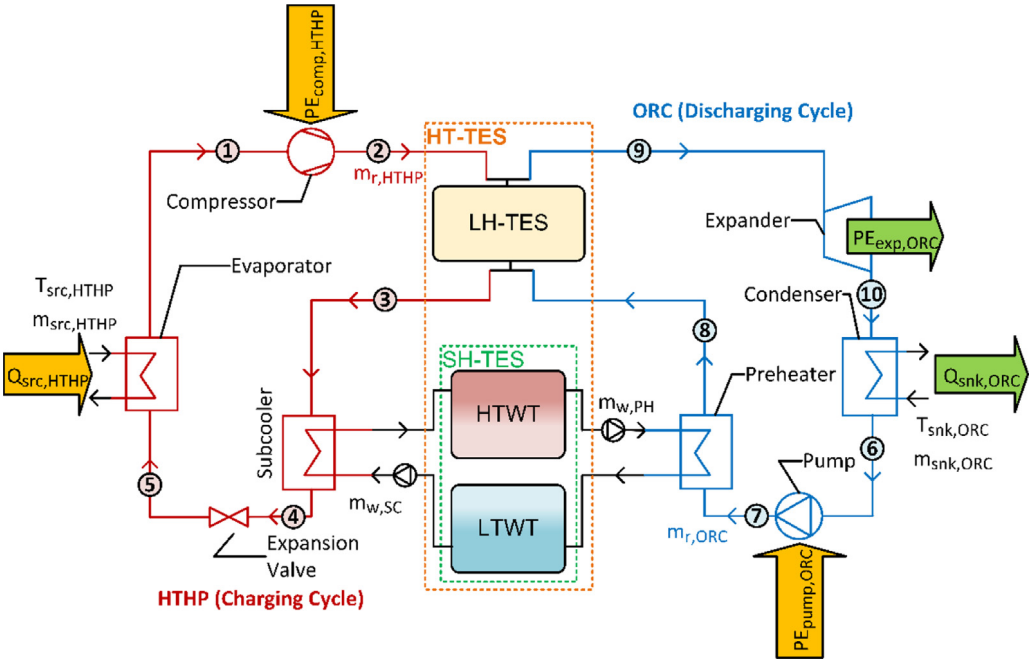

Fig. 1. Scheme of the CHEST system.

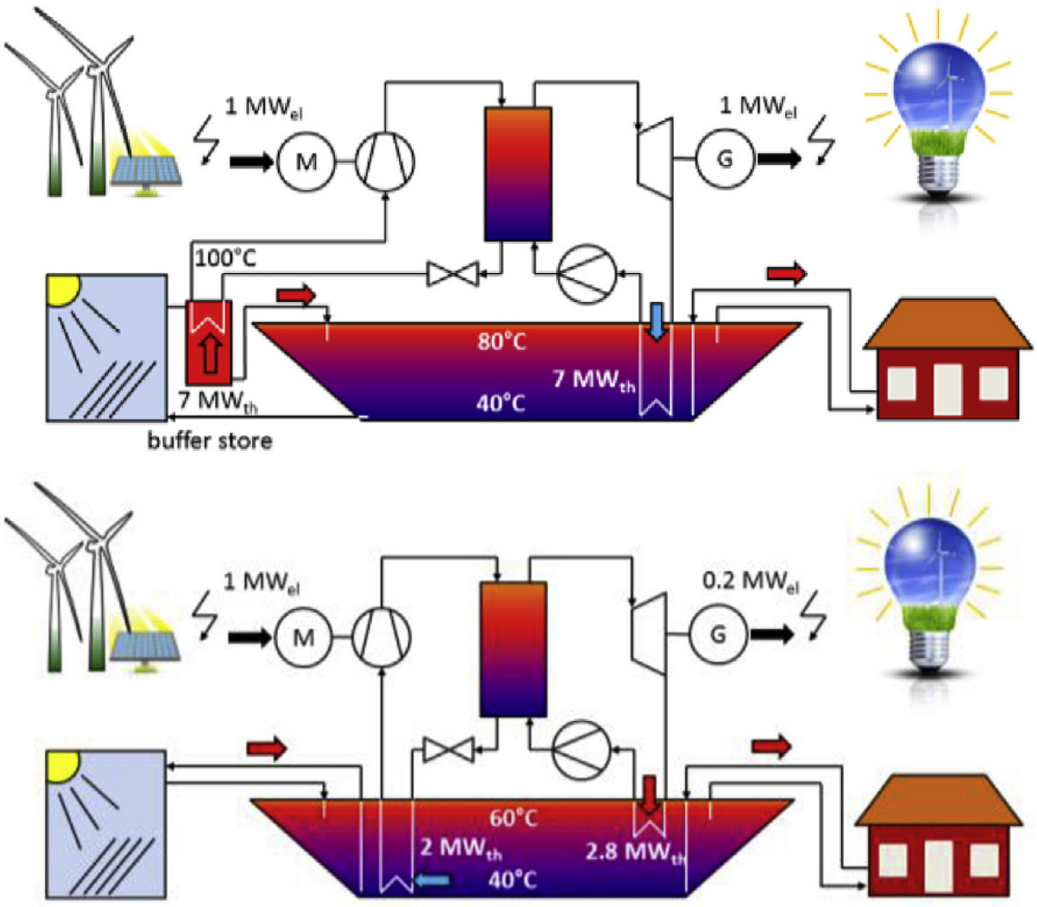

Fig. 2. CHEST system integrated with SDH: (up) summer mode, and (down) winter mode (Steinmann et al., 2019).

Table 1
The main performance parameters for HTHP.

Coefficient of performance (COP_{HTHP})	$= \frac{Q_{tot,HTHP}}{PE_{comp,HTHP}}$	[–]
Pressure ratio (Pr_{HTHP})	$= \frac{P_2}{P_1}$	[–]
Discharge temperature ($T_{dis,HTHP}$)	$= T_2$	[°C]
Volumetric heating capacity (VHC_{HTHP})	$= \frac{1}{v_1}(h_2 - h_4)$	[J m^{-3}]

where $h_{2,is}$ is the isentropic enthalpy at the exit of compressor.

The total heat ($Q_{tot,HP}$) provided by the HTHP during the charging process is:

$$Q_{tot,HTHP} = m_{r,HTHP}\,(h_2 - h_4) \tag{3}$$

The main performance parameters for the HTHP are defined in Table 1.

2.1.2. ORC analysis

ORCs are based on the Rankine steam cycle. However, instead of using water as the working fluid, they employ organic fluids which are characterized by a higher molecular mass and a lower boiling point compared with water. ORCs are mainly used for industrial waste heat-to-power applications. These applications are characterized by low temperatures (<350 °C) and low heat contents (Lecompte et al., 2015).

The ORC's refrigerant mass flow rate ($m_{r,ORC}$) is obtained based on the energy balance between charging and discharging cycles, assuming no heat losses.

$$Q_{tot,ORC} = Q_{tot,HTHP} = m_{r,ORC}\,(h_9 - h_7) \tag{4}$$

The output electrical power ($PE_{exp,ORC}$) from the expander is expressed in Eq. (5), taking into account the total expander efficiency $\eta_{tot,exp,ORC}$.

$$PE_{exp,ORC} = m_{r,ORC}\left(h_9 - h_{10,is}\right)\left(\eta_{tot,exp,ORC}\right) \tag{5}$$

where $h_{10,is}$ is the isentropic enthalpy at the exit of the expander.

The condenser capacity, or the heat rejected to the heat sink reservoir, is obtained as follows:

$$Q_{snk,ORC} = m_{r,ORC}\,(h_{10} - h_6) = m_{snk,ORC} \cdot Cp_{snk,ORC} \cdot \Delta T_{snk,ORC} \tag{6}$$

Finally, the electrical power input to the ORC's pump is expressed as follows:

$$PE_{pump,ORC} = \frac{m_{r,ORC}\left(h_{7,is} - h_6\right)}{\eta_{tot,pump,ORC}} \tag{7}$$

where $h_{7,is}$ is the isentropic enthalpy at the outlet of pump and $\eta_{tot,pump,ORC}$ is the total pump efficiency.

The most important performance parameter for the ORC in the current study is the thermal efficiency ($\eta_{th,ORC}$), which can be calculated as:

$$\eta_{th,ORC} = \frac{PE_{net,ORC}}{Q_{tot,ORC}} = \frac{PE_{exp,ORC} - PE_{pump,ORC}}{Q_{tot,ORC}} \tag{8}$$

Finally, to assess the global performance for the proposed CHEST system, the net power ratio (φ) is calculated as seen in Eq. (9). It is the ratio between the net output power from the ORC ($PE_{net,ORC}$) and input electrical power to the HTHP's compressor ($PE_{comp,HTHP}$). It is worth mentioning that the electrical power consumed by auxiliary equipment is neglected in the current work.

$$\varphi = \frac{PE_{net,ORC}}{PE_{comp,HTHP}} \tag{9}$$

Table 2
Thermal properties of selected PCMs (Pereira da Cunha and Eames, 2016).

Material	$T_{melt,PCM}$ [°C]	$\Delta h_{fs,PCM}$ [J kg^{-1}]
$LiNO_3$–KNO_3	133	150×10^3
KNO_2-$NaNO_3$	149	124×10^3
HCOONa–HCOOK	176	175×10^3

2.2. Heat storage medium

As indicated before, the heat storage medium is divided into a LH-TES and SH-TES systems. This separation allows, as stated by Steinmann (2017), for a better matching between the temperature profiles inside each heat exchanger, improving the heat transfer processes within the system. This HT-TES system behaves in a way such that the ratio between the sensible and latent heat is equal for both charging and discharging processes. Thus, the level of charge of both systems is the same under any circumstance. Furthermore, in this model the charges and discharges are always complete. So far, no heat losses in the HT-TES have been included, since the aim is to obtain the potential limit of the pumped thermal storage system.

2.2.1. LH-TES system configuration

The LH-TES system consists of a bundle of vertical finned-tubes surrounded by a phase change material (PCM). The fins can have a wide variety of shapes such as annular, plate, or branched (Weller et al., 2019). This system acts as the condenser for the HTHP and as the evaporator for the ORC. During the charging process, the HTHP's working fluid is condensed and the PCM is converted from solid to liquid. Assuming an ideal heat transfer process, the latent heat absorbed by the LH-TES system is:

$$Q_{lat,HTHP} = m_{r,HTHP}\,(h_2 - h_3) \tag{10}$$

In the discharging process, the refrigerant inside the ORC is evaporated, extracting heat from the solidification process of the PCM:

$$Q_{lat,ORC} = Q_{lat,HTHP} = m_{r,ORC}\,(h_9 - h_8) \tag{11}$$

In order to assess the potential performance of the system in a wide range of temperatures and applications, three different eutectic mixtures have been considered. The selected PCMs are listed in Table 2 and present high specific melting enthalpies and a very uniform phase-change temperature. The present work is nevertheless only a thermodynamic evaluation of the system performance for different potential storage temperatures, and not a detailed thermo-physical analysis of PCMs.

2.2.2. SH-TES system configuration

The SH-TES system is comprised of two pressurized tanks filled with water at two different temperature levels. The water contained in these tanks is used as a secondary fluid in the subcooler of the HTHP and in the preheater of the ORC. As a realistic example, the CHEST system prototype of 10 kWe, the experimental system intended to be tested during 2020–2021, In the charging process, the water, which flows from the low temperature water tank (LTWT), is heated up by means of the subcooling of the HTHP's refrigerant and is sent to the high temperature water tank (HTWT). The sensible heat exchanged in this process is:

$$Q_{sen,HTHP} = m_{r,HTHP}\,(h_3 - h_4) = m_{w,SC} Cp_{w,SC}(T_{w,SC,out} - T_{w,SC,in}) \tag{12}$$

For the discharge process, water from the HTWT is sent to the preheater of the ORC, cooled down and stored in the LTWT. The sensible heat transferred is:

$$Q_{sen,ORC} = Q_{sen,HTHP} = m_{r,ORC}\,(h_7 - h_6) = m_{w,PH} Cp_{w,PH}(T_{w,PH,in} - T_{w,PH,out}) \quad (13)$$

The European project CHESTER (grant agreement No. 764042) aims to build and test during 2020–2021 a first-of-its kind CHEST prototype of 10 kWe. The latter will have a brazed-plate subcooler and a preheater with maximum capacities of around 41 and 77 kW, respectively (De Paepe et al., 2019; Hassan et al., 2019).

As no heat losses are analysed for the SH-TES system, the temperature of the water contained in the SH-TES tanks is equal to the temperature of the water leaving the subcooler for the HTWT and the preheater for the LTWT. Regarding the values of these temperatures, that of the HTWT will be close to the PCM's melting temperature, and the LTWT's temperature is adjusted according to the boundary conditions of the system so as to have the same sensible to latent rates for charge and discharge.

2.3. Working fluids

Selecting the proper working fluid is crucial for the system performance, especially for the HTHP. One important aspect of selecting a refrigerant for the HTHP is the required degree of superheating (SH) after evaporation. Low SH values could result in wet compression, while high values could decrease the evaporation temperature and significantly affect the system performance. Regarding this, the refrigerants could be classified into three main groups based on the slope of saturated vapour curve on the T-s diagram (dT/ds). The negative slope refrigerants are called "wet fluids", the positive slope ones are called "dry fluids", and semi-vertical saturation curve ($dT/ds \gg 0$) refrigerants are called "isentropic fluids" (Jockenhöfer et al., 2018). Fig. 3 compares between three different refrigerants, one corresponding to each group.

As inferred from Fig. 3, wet fluids do not require any SH, or a very small value. Dry fluids need a very high degree of SH to prevent wet compression, which can significantly decrease the evaporation temperature, if it is done inside the evaporator, hereby hindering the COP_{HTHP} and the global system performance (Corberán et al., 2019). Another way to achieve this high value of SH is by employing an extra thermal heat storage, however this will increase the system complexity and also the irreversibilities associated with the heat transfer (Jockenhöfer et al., 2018). Isentropic fluids need a moderate degree of SH that could be done inside the evaporator without significant side effects on the system performance.

Other desirable criteria for selecting the refrigerant for the proposed system are: zero Ozone Depletion Potential (ODP = 0); very low Global Warming Potential (GWP < 10); non-toxic; no or low flammability; high critical temperature (T_{crit} > 145 °C) to work under subcritical conditions and a low critical pressure (P_{crit} < 3 MPa) (Arpagaus et al., 2018).

Table 3 Shows the most relevant thermal, environmental, and safety properties for different refrigerants which could be used for high temperature applications such as in the CHEST system. The thermal properties have been obtained from the Refprop 10 (Lemmon et al., 2018) and Engineering Equation Solver (EES) (Klein, 2019) databases.

Based on Table 3, water might seem to be a potential candidate. However, water has a low vapour density and it requires complicated multi-stage compression cycles given the high values of pressure ratio and discharge temperature (Steinmann, 2014). Such cycles are out of scope of the present work, so water has been excluded from the study. Another candidate is Acetone, which is also considered as a wet fluid. Corberán et al. (2019) reported that Acetone can reach a theoretical COP of 4.14 when employed in a HTHP with a temperature lift up to 80 K. The authors reported that, although Acetone has a very good theoretical performance, it lacks of experimental testing to support its potential use and reliability in such applications.

In the current study, the dry fluids (R-1336mzz(Z) and R-365mfc) were eliminated because, as mentioned before, they require very high SH values in the HTHP's evaporator to avoid wet compression, which leads to a degradation in the system performance.

The candidates with the most potential for the CHEST system are the refrigerants related to the isentropic fluids group (R-1233zd(E), R-1234ze(Z), R-245fa, Butene, and R-141b). Their main advantages include high VHC, low compression work and discharge temperature (Arpagaus et al., 2018; Corberán et al., 2019). R-1233zd(E) is considered to be an environmental-friendly replacement to R-245fa, which has a high GWP value of 858. Moreover, it has a higher critical temperature. Although, R-141b has a GWP of 782, it has been selected because it is the only refrigerant in this group that can reach the required high condensation temperatures for the HTHP (>150 °C).

Fig. 4 illustrates the temperature range (the difference between the critical temperature and normal boiling point) for the refrigerants selected for CHEST system simulations, alongside the expected limits, in the current study, for the HTHP's condensation temperature ($T_{cond,HTHP}$).

The condensation temperatures were assumed to be 5 K higher than the PCM melting temperatures. From Fig. 4 and Table 2, R-1233zd(E), R-1234ze(Z), and Butene seem to be the best candidates for $T_{melt,PCM}$ = 133 °C ($LiNO_3$–KNO_3). Regarding $T_{melt,PCM}$ = 149 °C (KNO_2-$NaNO_3$), Acetone, R-141b, and R-1233zd(E) are considered to be the best working fluids for the CHEST system. Finally, for $T_{melt,PCM}$ = 176 °C (HCOONa–HCOOK), Acetone and R-141b are the only refrigerants that can reach this limit.

3. Modelling approach and validation

The proposed CHEST system (Fig. 1) has been modelled using the program EES (Klein, 2019). This simulation tool has many advantages such as the modelling simplicity, fast calculation time, an extensive database of thermophysical properties for a vast number of working fluids, many optimization methods and detailed representation of thermodynamic cycles such as in P-h and T-s diagrams.

3.1. Modelling assumptions

The assumptions adopted for the proposed EES-CHEST model are:

- The system always works under steady state conditions.
- The auxiliary power consumption was neglected, except for the ORC's main feeding pump, since the work aims to assess the potential thermodynamic performance of the system.
- No heat losses in the HT-TES system.
- The PCM always melts and solidifies homogeneously at constant temperature equal to $T_{melt,PCM}$.
- The ratios of sensible to latent heat during charging and discharging are equal; this means that all the heat stored by the HTHP is consumed by the ORC with the same ratio.
- The inlet to the HTHP's subcooler and the outlet from the ORC's condenser is always saturated liquid.
- The water-side pressure drop values inside the HTHP's evaporator and subcooler and ORC's condenser and preheater are neglected.
- The refrigerant-side pressure drop values in the HTHP's subcooler and ORC's preheater are neglected.

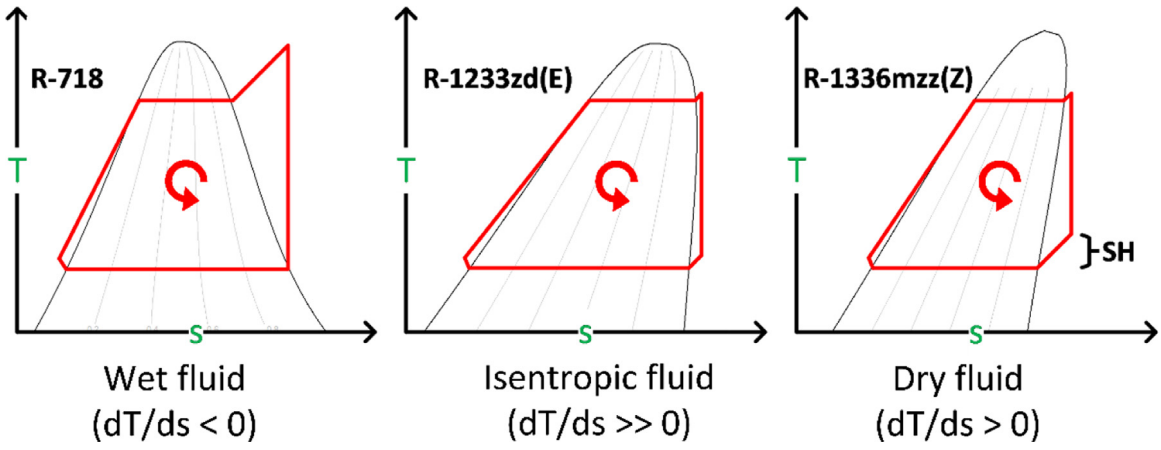

Fig. 3. Schematic of HTHP's cycle on a T-s diagram for different types of refrigerant.

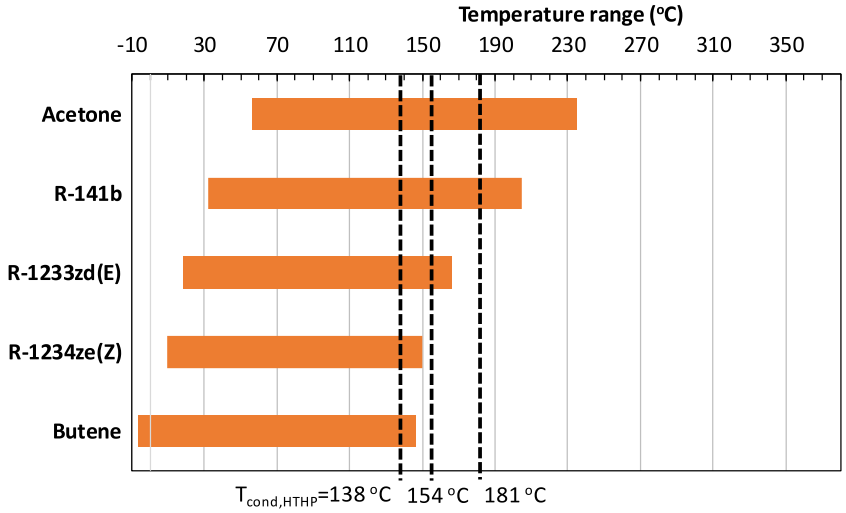

Fig. 4. Temperature ranges of the selected refrigerants for the CHEST system and expected HTHP's condensation temperatures.

Table 3
Properties of potential refrigerants for pumped thermal storage applications.

Group	Refrigerant	Type	T_{crit} [°C]	P_{crit} [MPa]	NBP[a] [°C]	ODP [–]	GWP [–]	SG[b]	$\rho_{sat,suc}$[c] [kg m^{-3}]
Wet	R-718 (water)	Natural	373.95	2.206	100.0	0	0	A1	0.29
	Acetone	HC[d]	235.0	4.7	56.0	0	<10	n.a.	4.60
Dry	R-1336mzz(Z)	HFO[e]	171.4	2.9	33.4	0	2	A1	27.47
	R-365mfc	HFC[f]	186.85	3.266	40.2	0	804	A2	19.89
Isentropic	R-1233zd(E)	HCFO[g]	166.5	3.62	18.3	0.0003	<1	A1	34.76
	R-1234ze(Z)	HFO	150.1	3.53	9.7	0	<1	A2L	42.21
	R-245fa	HFC	154.0	3.65	15.0	0	858	B1	44.12
	Butene	HC	146.15	4.0	−6.3	0	<10	n.a.	29.41
	R-141b	HCFC[h]	204.35	4.212	32.05	0.11	782	A1	18.77

[a]NBP: normal boiling point at 0.1013 MPa.
[b]SG: safety group (ASHRAE, 2016).
[c]Saturated suction density at 80 °C.
[d]HC: hydrocarbons.
[e]HFO: hydrofluoroolefins.
[f]HFC: hydrofluorocarbons.
[g]HCFO: hydrochlorofluoroolefins.
[h]HCFC: Hydrochlorofluorocarbons.

3.2. Validation of EES-CHEST model

Given that there is still no experimental installation of the CHEST concept, the developed model has been validated with a similar model from literature proposed by Jockenhöfer et al. (2018). The main validation parameter is the gross power ratio ($\varphi_{,gross}$) for a CHEST system using Butene as the working fluid. The subscript "gross" refers to the upper performance limit, since the power ratio is calculated as the total electrical power delivered by the ORC's expander divided by the total power consumed by the HTHP's compressor. The validation is shown for two sink

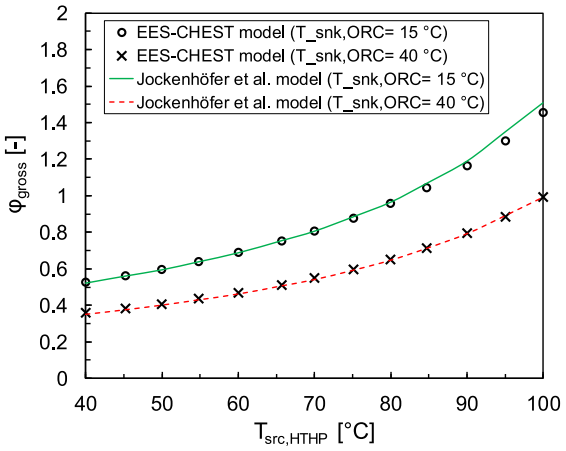

Fig. 5. Comparison of gross power ratio (φ_{gross}) values between the current EES-CHEST model and that proposed by Jockenhöfer et al. (2018).

temperatures ($T_{snk,ORC}$) of 15 and 40 °C, and the source temperature ($T_{src,HTHP}$) have been varied from 40 to 100 °C. For a fair comparison, the same assumptions, efficiencies and values of pressure drops and pinch points have been adopted as shown in Table 3 in Jockenhöfer et al. (2018). Fig. 5 shows that the EES-CHEST model predicts very well the φ_{gross} values compared to the model proposed by Jockenhöfer et al. The mean absolute deviation (MAD) in the results were ±1.245% and ±1.41% for $T_{w,snk,in}$ equals 15 and 40 °C, respectively.

4. Results and discussion

In this section, different parametric studies have been performed to obtain the potential performance of the CHEST system in a wide range of temperatures. The main analysis considers the use of a single working fluid in both the HTHP and ORC. However, at the end of the study, the possibility of using a different working fluid in the ORC's cycle has also been addressed.

For all the simulations, the fixed inputs to the model, regardless of the refrigerant, are listed in Table 4. The source temperature ($T_{src,HTHP}$) has been varied from 40 to 100 °C, and three sink temperatures ($T_{snk,ORC}$) have been simulated at 10, 25, and 40 °C. These values of source and sink temperatures have been selected to ensure a flexible CHEST system which can be easily integrated with different RES and seasonal pit water heat storage systems (Steinmann et al., 2019).

4.1. Effect of refrigerant state at the outlet of orc's preheater and excess heat rejection on the CHEST system performance

In the model developed by Jockenhöfer et al. (2018), the outlet from the ORC's preheater was always constrained as saturated liquid (Point 8). An extra heat exchanger was also employed to reject some excess heat (Q_{ex}) and to ensure a minimum degree of subcooling at the inlet of the HTHP's evaporator, especially at low source temperatures and high sink temperatures. This could prevent the generation of flash gas during the expansion process and ensure better distribution of the refrigerant at the inlet of the HTHP's evaporator. From a practical point of view, this is the most feasible solution, however, theoretically, it constrains the system and could result in a lower power ratio.

To understand this issue better, Fig. 6 shows the results for two CHEST system configurations using Butene as the working fluid. In the Config. 1 (Fig. 6a) there is no excess heat rejected and the EES-CHEST model was optimized to find the maximum power ratio regardless of the state of Point 8. Config. 2 (Fig. 6b) accounts for the excess heat rejection to ensure a minimum subcooling of 3 K at the inlet of the HTHP's evaporator. In this configuration, the EES-CHEST model was optimized to calculate the power ratio ensuring that Point 8 is always saturated liquid. For $T_{src,HTHP} = 40$ °C, $T_{snk,ORC} = 10$ °C, and $T_{melt,PCM} = 133$ °C, Fig. 6 shows that with no excess heat (Config. 1) the power ratio is improved by 7.7%.

Fig. 7 shows the parametric study done to compare between the two configurations for sink temperatures of 10 and 40 °C, considering the whole range of source temperatures. The power ratio of the CHEST system in the case of Config. 1 (no Q_{ex}) is always higher than that of Config. 2 (with Q_{ex}). The results showed, within the range of study, that Config. 1 (no Q_{ex}) has φ values higher than Config. 2 (with Q_{ex}) by 7.9% and 8.4%, in average, for sink temperatures of 10 and 40 °C, respectively.

As the main objective of the current work is to assess the theoretical performance and the maximum benefits from the CHEST system, and based on the previous results, Config. 1 was found to be more adequate for the next study comparing the impact of employing different refrigerants and PCM melting temperatures.

Table 4
Input fixed parameters to the EES-CHEST model.

Parameter	Unit	Value	Comments
$PE_{comp,HTHP}$	MW	1	Total electrical power input to the HTHP's compressor.
ΔT_{PP}	K	5	Pinch point approach in all heat exchangers.
$\Delta T_{src,HTHP}$	K	5	Water-side temperature lift inside the HTHP's evaporator.
$\Delta T_{snk,ORC}$	K	5	Water-side temperature lift inside the ORC's condenser.
$SH_{evap,HTHP}$	K	5	Superheat inside the HTHP's evaporator.
$SH_{LH-TES,ORC}$	K	5	Superheat inside the ORC's LH-TES.
$\Delta T_{sat,evap,HTHP}$	K	2	Saturation temperature drop inside the HTHP's evaporator.
$\Delta T_{sat,LH-TES,HTHP}$	K	0.5	Saturation temperature drop inside the LH-TES (HTHP-side).
$\Delta T_{sat,LH-TES,ORC}$	K	0.7	Saturation temperature drop inside the LH-TES (ORC-side).
$\Delta T_{sat,cond,ORC}$	K	1.5	Saturation temperature drop inside the ORC's condenser.
$\eta_{tot,comp,HTHP} = \eta_{tot,pump,ORC}$	–	0.75	Total efficiency of the HTHP's compressor and ORC's main pump.
$\eta_{is,comp,HTHP} = \eta_{is,pump,ORC}$	–	0.8	Isentropic efficiency of the HTHP's compressor and ORC's main pump.
$\eta_{tot,exp,ORC}$	–	0.85	Total expander efficiency.
$\eta_{is,exp,ORC}$	–	0.88	Isentropic efficiency of the expander.

4.2. Comparison of the CHEST system performance for different refrigerants and PCM melting temperatures

In the current work, three different temperatures of $T_{melt,PCM}$ have been assessed (133, 149, and 176 °C). For each temperature level, different working fluids were compared and evaluated, assuming the same working fluid in both the HTHP and ORC. In a final stage (Section 4.3), different working fluids in the HTHP and ORC were simulated. The LH-TES is considered to be the HTHP's heat sink because it defines the required condensation temperature. This heat sink is assumed to be infinite in the model, with a constant temperature equal to $T_{melt,PCM}$.

A nominal point for the proposed CHEST system was selected to compare between different refrigerants. The nominal conditions are 80 °C for the HTHP's source temperature and 25 °C for the ORC's sink temperature. The HTHP's sink temperature varies based on PCM melting temperature.

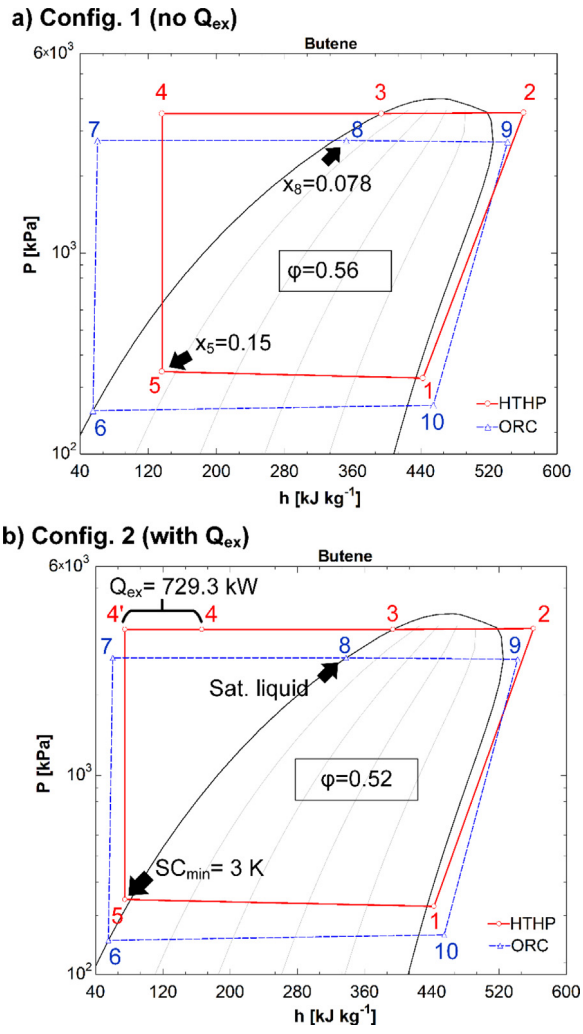

Fig. 6. P-h diagram of the CHEST system using Butene as the working fluid for two different configurations (without and with excess heat).

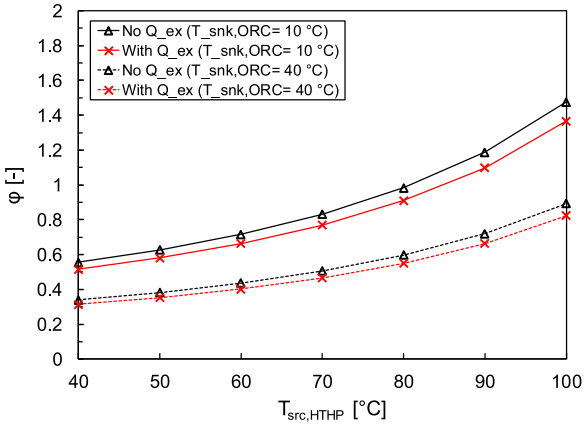

Fig. 7. Power ratio with and without excess heat.

4.2.1. PCM melting temperature = 133 °C

As explained before, the three candidates for this temperature level are R-1233zd(E), R-1234ze(Z), and Butene. For three ORC sink temperatures ($T_{snk,ORC}$ = 10, 25, and 40 °C), Fig. 8 shows the comparison of φ for $T_{src,HTHP}$ values from 40 to 100 °C.

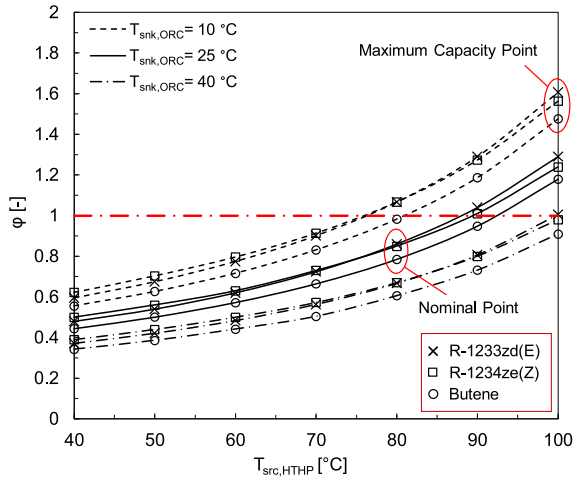

Fig. 8. Power ratio (φ) of the CHEST system for different refrigerants and $T_{melt,PCM}$ = 133 °C.

Generally, R-1233zd(E) gives the highest φ values, especially for $T_{src,HTHP}$ higher than 80 °C, compared with R-1234ze(Z) and Butene. Under the nominal conditions, R-1233zd(E) has a φ of 0.86, which is 1.2% and 8.9% higher than for R-1234ze(Z) and Butene, respectively. For the maximum capacity point, where $T_{src,HTHP}$ = 100 °C and $T_{snk,ORC}$ = 10 °C, R-1233zd(E) can reach φ of 1.61, which is higher by 3.2% and 8.8%, respectively, compared with R-1234ze(Z) and Butene.

However, the main problem with R-1233zd(E) is its high NBP value (18.3 °C). The results show that for $T_{snk,ORC}$ = 10 °C, the pressure inside the ORC's condenser could be very close to the atmospheric pressure. This could result in a risk of air infiltration to the cycle and degradation of the performance. The main disadvantage of Butene and R-1234ze(Z) is that they are flammable fluids, unlike R-1233zd(E) which is non-flammable.

Regarding the HTHP's performance at this temperature level, Fig. 9 shows the values of COP_{HTHP}, Pr_{HTHP}, VHC_{HTHP}, and $T_{dis,HTHP}$ for the three refrigerants, under the range of $T_{src,HTHP}$ and with a fixed $T_{snk,ORC}$ of 25 °C.

The COP_{HTHP} curves for the three refrigerants present a similar trend as those for the φ; R-1233zd(E) has the highest COP_{HTHP} values, especially for $T_{src,HTHP}$ higher than 70 °C. At the nominal point, a COP_{HTHP} of 5.92 can be reached, compared to 5.83 for R-1234ze(Z) and 5.56 for Butene. Fig. 9a shows that Butene is the only refrigerant that can reach the lowest $T_{src,HTHP}$ (≈42.5°C) with $Pr_{HTHP} \leq 10$, which is considered, in the current work, as the limit for single-stage compression cycle. This pressure ratio limit was set based on the correlation proposed by Navarro-Peris et al. (2013), assuming a minimum theoretical volumetric efficiency of 0.35. Regarding the VHC_{HTHP}, Butene shows the highest values; it can reach a VHC_{HTHP} value of 13.11 MJ m^{-3} at $T_{src,HTHP}$ = 100 °C, compared with 11.35 MJ m^{-3} for R-1234ze(Z) and 9.11 MJ m^{-3} for R-1233zd(E). Under these conditions, this means that to pump 1 MJ using Butene as the working fluid, the compressor size required, in m^3, is smaller than the one used for R-1234ze(Z) and R-1233zd(E) by 13.64% and 31%, respectively.

Only R-1233zd(E) and Butene have $T_{dis,HTHP}$ values much lower than the specified limit, which is set at 160 °C, for the whole range of $T_{src,HTHP}$. The maximum discharge temperature limit was selected referring to the technical specifications of the Viking Heat Engines' compressor (HBC 511) (Viking Heat Engines, 2018), which is considered to be one of the most robust industrial compressors in the market nowadays. R-1234ze(Z), Butene, and

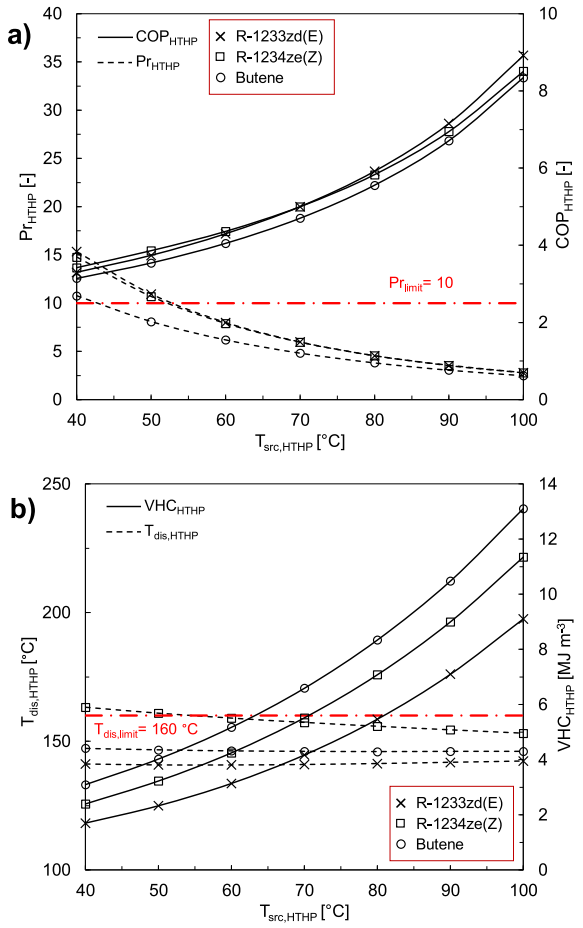

Fig. 9. HTHP's performance for $T_{melt,PCM}$ = 133 °C and $T_{snk,ORC}$ = 25 °C.

R-1233zd(E) have average values of $T_{dis,HTHP}$ of 157.70, 146.37, and 141.34 °C, respectively.

Considering the $\eta_{th,ORC}$, for the nominal conditions, R-1234ze(Z) has the highest $\eta_{th,ORC}$ value of 0.15, compared with 0.14 for both Butene and R-1233zd(E).

4.2.2. PCM melting temperature = 149 °C

At this intermediate temperature level, the pre-selected refrigerants are Acetone, R-141b, and R-1233zd(E). Fig. 10 shows the φ values for the mentioned refrigerants under the selected range of source and sink temperatures.

Fig. 10 indicates that both Acetone and R-141b have nearly identical performance regarding the φ. Under the nominal conditions, they have an φ of approximately 0.87, which is higher than that of R-1233zd(E) by 11.5%. However, under the maximum capacity conditions, this difference reduces to be only 6%.

The main undesirable properties of R-141b are the high GWP (=782) and NBP (=32.05 °C) values. Acetone also has a very high NBP value of 56 °C, besides being a highly flammable fluid. Using Acetone in the ORC always results in a negative pressure inside the ORC's condenser for the given range of ORC's sink temperatures. The same problem appears when using R-141b as a working fluid, but only if $T_{snk,ORC}$ = 10 °C.

Fig. 11a shows that R-141b has the highest COP_{HTHP} values, with a nominal COP_{HTHP} of 5.12, compared with 4.91 for both Acetone and R-1233zd(E). Both R-141b and R-1233zd(E) can work with Pr_{HTHP} values $\leq$ 10 for the $T_{src,HTHP}$ range of 63–100 °C, approximately. Acetone, on the other hand, can work under this Pr_{HTHP} limit from $T_{src,HTHP} \approx$ 74.5 to 100 °C.

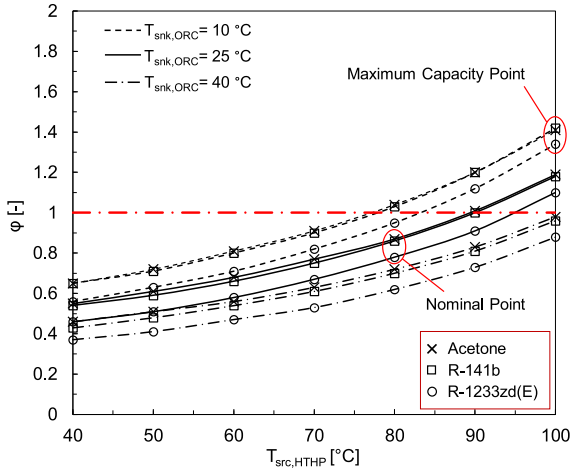

Fig. 10. Power ratio of the CHEST system for different refrigerants and $T_{melt,PCM}$ = 149 °C.

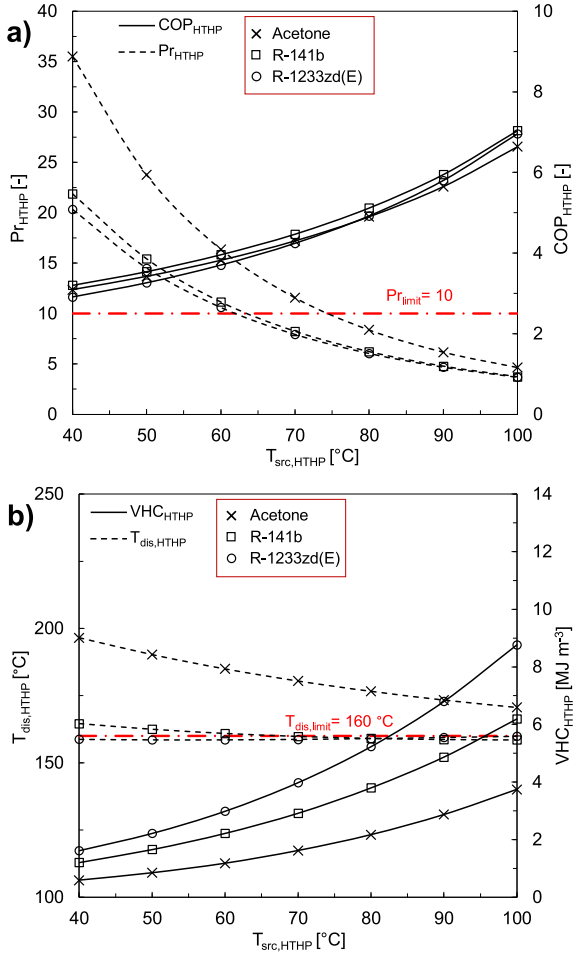

Fig. 11. HTHP's performance for $T_{melt,PCM}$ = 149 °C and $T_{snk,ORC}$ = 25 °C.

Based on Fig. 11b, R-1233zd(E) has the highest VHC_{HTHP} values within the whole range of $T_{src,HTHP}$. It can reach a maximum VHC_{HTHP} value of 8.76 MJ m^{-3}. This is substantially higher than that for Acetone and R-141b by 134% and 41.5%, respectively. At this temperature level, Acetone always have $T_{dis,HTHP}$ values much higher than the specified maximum limit of 160 °C, with

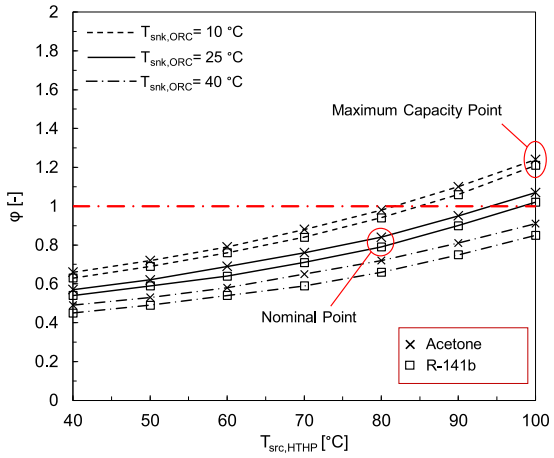

Fig. 12. Power ratio of the CHEST system for different refrigerants and $T_{melt,PCM}$ = 176 °C.

an average value of 182 °C. On the other hand, R-141b and R-1233zd(E) have $T_{dis,HTHP}$ values very close to the maximum limit with average values of 161 and 159 °C, respectively.

Under the nominal point, Acetone shows the highest $\eta_{th,ORC}$ of 0.18, compared with R-141b, which has $\eta_{th,ORC}$ = 0.17, and R-1233zd(E), which has $\eta_{th,ORC}$ = 0.16.

4.2.3. PCM melting temperature = 176 °C

The choices are limited to only Acetone and R-141b for this high temperature level. Fig. 12 shows that Acetone generally has the highest φ values compared with R-141b. For the nominal point, φ is equal to 0.84, which is higher than that of R-141b by 6.3%. Regarding the maximum capacity point, Acetone can reach a φ of 1.24, which is higher by 2.5% than that of R-141b.

However, as mentioned before, using Acetone in the ORC results in a negative pressure inside the ORC's condenser due to its high NBP. $T_{snk,ORC}$ has to be at least 60 °C to avoid this phenomenon.

Fig. 13a shows that the functionality of a single-stage compression cycle within this high temperature level is very limited due to the exponential increase of Pr_{HTHP} for decreasing $T_{src,HTHP}$ values in both refrigerants. The results showed that R-141b should work between $T_{src,HTHP} \approx$ 82 to 100 °C to have a $Pr_{HTHP} \leq 10$, while Acetone is very limited to a $T_{src,HTHP}$ range approximately from 90 to 100 °C only. Another challenge for the HTHP cycle is the very high $T_{dis,HTHP}$ values for the two refrigerants. Fig. 13b yields average $T_{dis,HTHP}$ values for Acetone and R-141b of 209 and 188 °C, respectively. These elevated temperatures can damage the compressor and deteriorate the lubrication system. These challenges imply that for this high temperature level of $T_{melt,PCM}$, multi-stage compression or cascade HTHP cycles are a must. However, this will lead to a complicated HT-TES system and an additional difficulty to match the temperature profiles during charging and discharging (Steinmann, 2014).

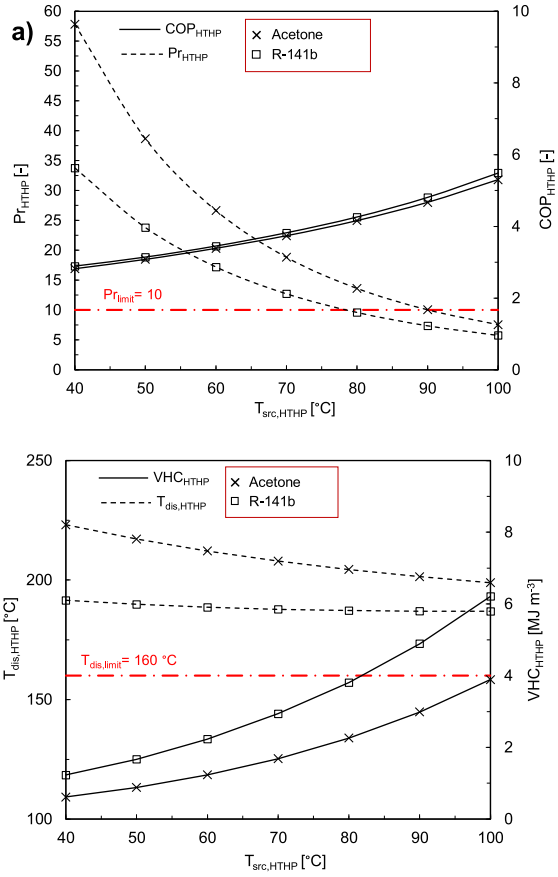

Fig. 13. HTHP's performance for $T_{melt,PCM}$ = 176 °C and $T_{snk,ORC}$ = 25 °C.

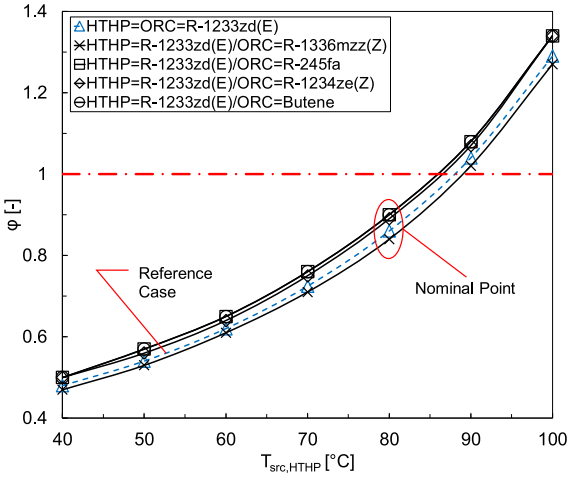

Fig. 14. Comparison of φ using R-1233zd(E) for the HTHP vs. different refrigerants for the ORC, for fixed $T_{melt,PCM}$ = 133 °C and $T_{snk,ORC}$ = 25 °C.

4.3. Employing a distinct working fluid in the ORC

In the previous section, the results showed that there are some working fluids that have fairly high NBP values, which can lead to a negative pressure inside the ORC's condenser under low values of $T_{snk,ORC}$, such as Acetone, R-141b, and R-1233zd(E). Therefore, in this section, different working fluids for the ORC are evaluated, keeping R-1233zd(E) as the main working fluid for the HTHP and fixing $T_{melt,PCM}$ to 133 °C and $T_{snk,ORC}$ to 25 °C. This also gives the opportunity to assess the performance of dry fluids, such as R-1366mzz(Z), which are difficult to employ in the HTHP cycle due to the high SH values required inside the HTHP's evaporator.

Fig. 14 shows that the performances, regarding φ, of R-245fa and Butene are the highest compared to other fluids, and are nearly identical. For the nominal point, both fluids have φ = 0.9, which is higher by 4.7% compared with the reference case which employs R-1233zd(E) as the working fluid for both the HTHP and ORC. R-245fa and Butene reach the maximum φ of 1.34 at

$T_{src,HTHP}$ = 100 °C. This is higher than that of the reference case by 3.9%. Although, R-245fa has a very good performance for the ORC, it is under phase-down recently due to its high GWP (= 858). Unlike R-245fa, Butene is a natural fluid that has very low GWP and NBP values, which makes it very suitable for the ORC.

Using R-1234ze(Z) in the ORC shows a similar behaviour as R-245fa and Butene with slightly lower φ values. Compared with the reference case, it has a higher nominal φ by 3.5%.

The dry fluid R-1336mzz(Z) has the lowest performance compared to the others. Under the nominal conditions, it reaches $\varphi = 0.84$, which is lower than the reference case by 2.33%.

Fig. 15 shows the CHEST system performance under nominal conditions using R-1233zd(E) for the HTHP, while Butene is utilized in the ORC. For 1 MW electrical power input to the HTHP's compressor, the system absorbs 5.42 MW from the HTHP's heat source, to store a total thermal power of 6.20 MW in the HT-TES system. Later, the stored heat is used by the ORC to produce a net electrical power of 0.90 MW, while 5.43 MW is rejected to the ORC's heat sink. The refrigerant mass flow rates inside the HTHP and ORC are 27.1 and 14.22 kg s^{-1} respectively. Theoretically, using two different refrigerants for the HTHP and ORC is considered to be a good solution to optimize the CHEST system. However, practically, this could complicate the design of the LH-TES, as each cycle needs a separate path to prevent the migration of refrigerant charge and lubricant oil between the two cycles.

5. Conclusions and future developments

In this paper, a thermodynamic model of a compressed heat energy storage system (CHEST) has been developed using EES. The model has been validated with published literature, with a maximum MAD of ±1.4%. A special emphasis has been placed on maximizing the advantage of the refrigerant subcooling.

Different parametric studies have been performed, assuming a 1 MW electrical power input to the HTHP, to compare different system configurations, refrigerants, and PCM melting temperatures (HTHP's heat sink). The main conclusions are:

- The authors have shown that the CHEST system configuration without excess heat rejection and with an unrestricted outlet from the ORC's preheater yields a better theoretical performance compared with the configuration that employs an extra heat exchanger for the excess heat and with fixed saturated liquid state at the outlet of the ORC's preheater. Using Butene as the working fluid and for the range of HTHP source temperatures studied, avoiding excess heat yields φ values that are, in average, 7.9% and 8.4% higher for ORC sink temperatures of 10 and 40 °C, respectively.
- For a PCM melting temperature of 133 °C, the results of using R-1233zd(E) or R-1234ze(Z) in both the HTHP and ORC show that they have a similar performance, higher than that of Butene. For the nominal point selected ($T_{src,HTHP}$ = 80 °C and $T_{snk,ORC}$ = 25 °C), R-1233zd(E) provides a power ratio φ of 0.86, which is 1.2% and 8.9% higher than that for R-1234ze(Z) and Butene, respectively. Regarding the HTHP performance at the nominal point, R-1233zd(E) has COP_{HTHP}, Pr_{HTHP}, VHC_{HTHP}, and $T_{dis,HTHP}$ values of 5.92, 4.56, 5.47 MJ m^{-3}, and 141.4 °C, respectively. R-1233zd(E) is considered to be one of the potential candidates for the CHEST system.
- For a PCM melting temperature of 149 °C, Acetone and R-141b show a nearly identical performance and higher values of φ compared to R-1233zd(E). For the nominal conditions, Acetone and R-141b have a φ of 0.87, which is higher than that of R-1233zd(E) by 11.5%. However, R-1233zd(E) has proved to be the best candidate at this temperature level considering in global the overall efficiency, flammability and pressure issues of the different studied refrigerants.

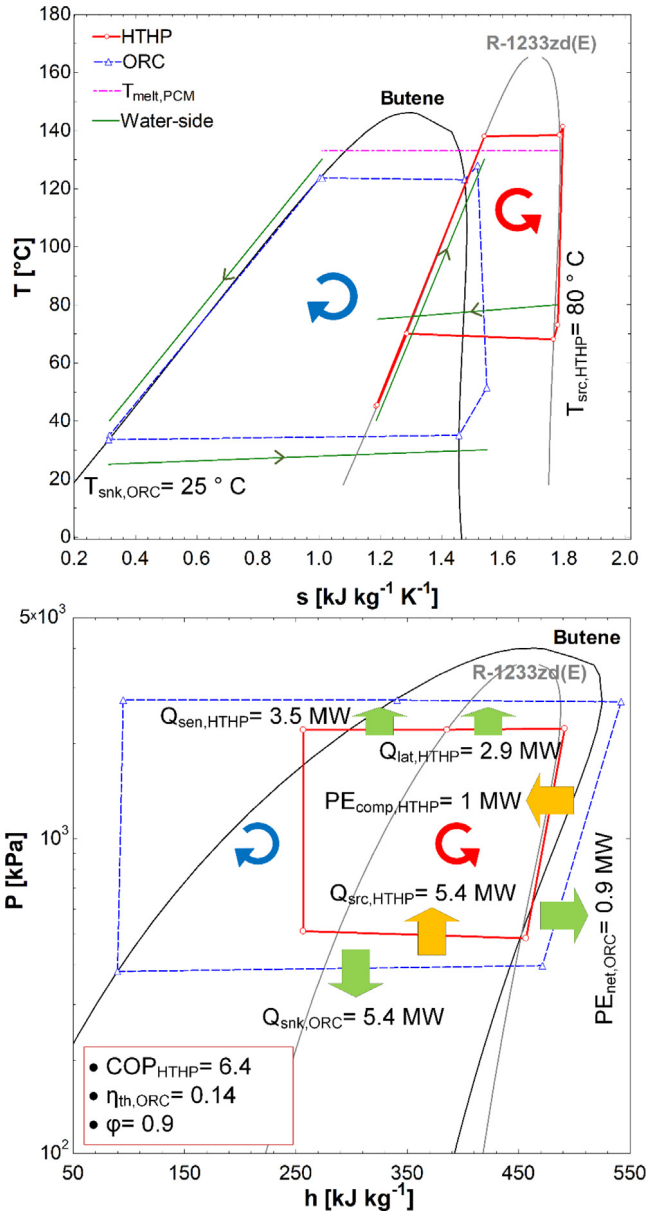

Fig. 15. T-s (up) and P-h (down) diagrams for CHEST system at nominal point and $T_{melt,PCM}$ = 133 °C using R-1233zd(E) for HTHP and Butene for ORC.

- For the highest PCM melting temperature of 176 °C, the only two suitable refrigerants are Acetone and R-141b. Under the nominal conditions, Acetone has a φ of 0.84, which is higher than that of R-141b by 6.3%. However, at this high temperature level, the CHEST system functionality is very limited due to the high values of Pr_{HTHP} (>10) and $T_{dis,HTHP}$ (>160 °C) that exceed the limits specified, in the current work, for single-stage HTHP. To operate the CHEST system under the full range of $T_{src,HTHP}$, a multi-stage compression or cascade cycle should be adopted for the HTHP.
- The possibility of using a different refrigerant in the ORC has also been investigated. Five different refrigerants for the ORC were compared, while maintaining R-1233zd(E) as the working fluid for HTHP, the PCM melting temperature of 133 °C, and the ORC sink temperature of 25 °C. The results show that the combination of R-1233zd(E) for the HTHP and Butene for the ORC is the best, regarding the φ. Under nominal conditions, this combination gives COP_{HTHP},

VHC_{HTHP}, Pr_{HTHP}, $\eta_{th,ORC}$, and φ values of 6.36, 5.88 MJ m^{-3}, 4.6, 0.14, and 0.9, respectively. The φ reaches a maximum value of 1.34 for $T_{src,HTHP} = 100$ °C.

The current work presents the full thermodynamic potential of a CHEST system assuming no thermal losses and neglecting the auxiliary power consumption. Furthermore, full charging and discharging processes have been assumed in the overall performance evaluation. The results of this work have been employed to assist in the design of the first-of-its-kind laboratory scale CHEST system, which, presumably, will be built during 2020. A dynamic model of the CHEST system is currently under development to evaluate the size of the thermal storage system, the required charging and discharging periods, and the consequent potential applications of the proposed system.

Declaration of competing interest

The authors declare that they have no known competing financial interests or personal relationships that could have appeared to influence the work reported in this paper.

Acknowledgement

This work has been partially funded by the grant agreement No. 764042 (CHESTER project) of the European Union's Horizon 2020 research and innovation program.

References

Abarr, M., Geels, B., Hertzberg, J., Montoya, L.D., 2017a. Pumped thermal energy storage and bottoming system part a: Concept and model. Energy 120, 320–331. http://dx.doi.org/10.1016/j.energy.2016.11.089.

Abarr, M., Hertzberg, J., Montoya, L.D., 2017b. Pumped thermal energy storage and bottoming system part b: Sensitivity analysis and baseline performance. Energy 119, 601–611. http://dx.doi.org/10.1016/j.energy.2016.11.028.

Aneke, M., Wang, M., 2016. Energy storage technologies and real life applications – A state of the art review. Appl. Energy 179, 350–377. http://dx.doi.org/10.1016/j.apenergy.2016.06.097.

Arpagaus, C., Bless, F., Uhlmann, M., Schiffmann, J., Bertsch, S.S., 2018. High temperature heat pumps: Market overview, state of the art, research status, refrigerants, and application potentials. Energy 152, 985–1010. http://dx.doi.org/10.1016/j.energy.2018.03.166.

ASHRAE, 2016. Standard 34-safety standard for refrigeration systems and designation and classification of refrigerants.

BP plc, 2018. BP Statistical Review of World Energy. London.

Budt, M., Wolf, D., Span, R., Yan, J., 2016. A review on compressed air energy storage: Basic principles, past milestones and recent developments. Appl. Energy 170, 250–268. http://dx.doi.org/10.1016/j.apenergy.2016.02.108.

Cheayb, M., Marin Gallego, M., Tazerout, M., Poncet, S., 2019. Modelling and experimental validation of a small-scale trigenerative compressed air energy storage system. Appl. Energy 239, 1371–1384. http://dx.doi.org/10.1016/j.apenergy.2019.01.222.

Corberán, J.M., Hassan, A.H., Payá, J., 2019. Thermodynamic analysis and selection of refrigerants for high-temperature heat pumps. In: Proceedings of the 25th IIR International Congress of Refrigeration. International Institute of Refrigeration, Montreal, Canada.

Pereira da Cunha, J., Eames, P., 2016. Thermal energy storage for low and medium temperature applications using phase change materials - A review. Appl. Energy 177, 227–238. http://dx.doi.org/10.1016/j.apenergy.2016.05.097.

De Paepe, M., Lecompte, S., Pillai, A., 2019. D3.4: Detailed Design of the ORC Laboratory Prototype. CHESTER Project, www.chester-project.eu.

European Comission, 2018. A Clean Planet for all. A European strategic long-term vision for a prosperous, modern, competitive and climate neutral economy. Brussels.

European Council, 2014. European Council 23/24 2014 - Conclusions. Brussels.

Fan, J., Xie, H., Chen, J., Jiang, D., Li, C., Ngaha Tiedeu, W., Ambre, J., 2020. Preliminary feasibility analysis of a hybrid pumped-hydro energy storage system using abandoned coal mine goafs. Appl. Energy 258, http://dx.doi.org/10.1016/j.apenergy.2019.114007.

Frate, G.F., Antonelli, M., Desideri, U., 2017. A novel pumped thermal electricity storage (PTES) system with thermal integration. Appl. Therm. Eng. 121, 1051–1058. http://dx.doi.org/10.1016/j.applthermaleng.2017.04.127.

Giovannelli, A., Tamasi, L., Salvini, C., 2019. Performance analysis of industrial steam turbines used as air expander in compressed air energy storage (CAES) systems. Energy Rep. 2, 2–25. http://dx.doi.org/10.1016/j.egyr.2019.08.066.

Guo, J., Cai, L., Chen, J., Zhou, Y., 2016. Performance optimization and comparison of pumped thermal and pumped cryogenic electricity storage systems. Energy 106, 260–269. http://dx.doi.org/10.1016/j.energy.2016.03.053.

Hassan, A.H., Corberán, J.-M., Sanchez, V., 2019. D3.2: Detailed Design of the High Temperature Heat Pump Laboratory Prototype. CHESTER project, www.chester-project.eu.

Jockenhöfer, H., Steinmann, W.D., Bauer, D., 2018. Detailed numerical investigation of a pumped thermal energy storage with low temperature heat integration. Energy 145, 665–676. http://dx.doi.org/10.1016/j.energy.2017.12.087.

Klein, S.A., 2019. Engineering equation solver (version v10.643).

Kusakana, K., 2019. Hydro aeropower for sustainable electricity cost reduction in South African farming applications. Energy Rep. 5, 1645–1650. http://dx.doi.org/10.1016/j.egyr.2019.11.023.

Laughlin, R.B., 2017. Pumped thermal grid storage with heat exchange. J. Renew. Sustain. Energy 9, http://dx.doi.org/10.1063/1.4994054.

Lecompte, S., Huisseune, H., van den Broek, M., Vanslambrouck, B., De Paepe, M., 2015. Review of organic rankine cycle (ORC) architectures for waste heat recovery. Renew. Sustain. Energy Rev. 47, 448–461. http://dx.doi.org/10.1016/j.rser.2015.03.089.

Lemmon, E.W., Bell, I.H., Huber, M.L., McLinden, M.O., 2018. NIST Standard reference database 23: Reference fluid thermodynamic and transport properties-REFPROP.

Liu, J.L., Wang, J.H., 2016. A comparative research of two adiabatic compressed air energy storage systems. Energy Convers. Manag. 108, 566–578. http://dx.doi.org/10.1016/j.enconman.2015.11.049.

Ma, T., Yang, H., Lu, L., 2014. Feasibility study and economic analysis of pumped hydro storage and battery storage for a renewable energy powered island. Energy Convers. Manag. 79, 387–397. http://dx.doi.org/10.1016/j.enconman.2013.12.047.

McTigue, J.D., White, A.J., Markides, C.N., 2015. Parametric studies and optimisation of pumped thermal electricity storage. Appl. Energy 137, 800–811. http://dx.doi.org/10.1016/j.apenergy.2014.08.039.

Navarro-Peris, E., Corberán, J.M., Falco, L., Martínez-Galván, I.O., 2013. New non-dimensional performance parameters for the characterization of refrigeration compressors. Int. J. Refrig. 36, 1951–1964. http://dx.doi.org/10.1016/j.ijrefrig.2013.07.007.

Steinmann, W.D., 2014. The CHEST (Compressed Heat Energy STorage) concept for facility scale thermo mechanical energy storage. Energy 69, 543–552. http://dx.doi.org/10.1016/j.energy.2014.03.049.

Steinmann, W.D., 2017. Thermo-mechanical concepts for bulk energy storage. Renew. Sustain. Energy Rev 75, 205–219. http://dx.doi.org/10.1016/j.rser.2016.10.065.

Steinmann, W.-D., Bauer, D., Jockenhöfer, H., Johnson, M., 2019. Pumped thermal energy storage (PTES) as smart sector-coupling technology for heat and electricity. Energy 183, 185–190. http://dx.doi.org/10.1016/j.energy.2019.06.058.

Taylor, P., Bolton, R., Stone, D., Zhang, X.-P., Martin, C., Upham, P., 2012. Pathways for Energy Storage in the UK. Cent. Low Carbon Futur. York.

Thess, A., 2013. Thermodynamic efficiency of pumped heat electricity storage. Phys. Rev. Lett. 111, 1–5. http://dx.doi.org/10.1103/PhysRevLett.111.110602.

Viking Heat Engines, 2018. HBC 511: Piston compressor for industrial heat pumps.

Weller, T., Jockenhöfer, H., Fiss, M., Bauer, D., 2019. D3.3: Detailed Design of the High Temperature TES Laboratory Prototype. CHESTER Project, www.chester-project.eu.